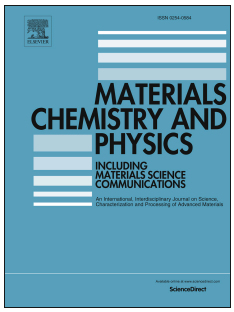

Composition dependence in surface properties of poly(lactic acid)/graphene/carbon nanotube composites

Radost Ivanova, Rumiana Kotsilkova, Evgeni Ivanov, Ricardo K. Donato, Guilhermino J.M. Fechine, Ricardo J.E. Andrade, Rosa di Maio, Clara Silvestre

PII: S0254-0584(20)30084-5

DOI: https://doi.org/10.1016/j.matchemphys.2020.122702

Reference: MAC 122702

To appear in: *Materials Chemistry and Physics*

Received Date: 1 August 2019

Revised Date: 16 January 2020

Accepted Date: 21 January 2020

Please cite this article as: R. Ivanova, R. Kotsilkova, E. Ivanov, R.K. Donato, G.J.M. Fechine, R.J.E. Andrade, R. di Maio, C. Silvestre, Composition dependence in surface properties of poly(lactic acid)/graphene/carbon nanotube composites, *Materials Chemistry and Physics* (2020), doi: https://doi.org/10.1016/j.matchemphys.2020.122702.

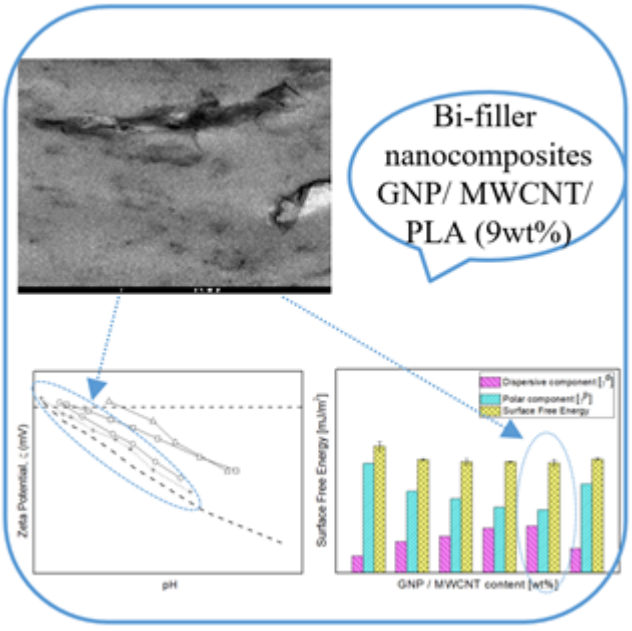

Composition dependence in surface properties of poly(lactic acid)/graphene/carbon nanotube composites

Radost Ivanova[1]*, Rumiana Kotsilkova[1], Evgeni Ivanov[1,2], Ricardo K. Donato[3], Guilhermino J. M. Fechine[4], Ricardo J. E. Andrade[4], Rosa di Maio[5], Clara Silvestre[5]

[1] *Open Laboratory on Experimental Micro and Nano Mechanics, Institute of Mechanics, Bulgarian Academy of Sciences, Acad. G. Bonchev Str., Block 4, Sofia, Bulgaria, r.ivanova@imbm.bas.bg (R.I.), kotsilkova@imbm.bas.bg (R.K.), ivanov_evgeni@imbm.bas.bg (E.I.)*

[2] *Research and Development of Nanomaterials and Nanotechnologies (NanoTech Lab Ltd.) Acad. G. Bonchev Str. Block 4, 1113 Sofia, Bulgaria, ivanov_evgeni@imbm.bas.bg (E.I.)*

[3] *Institute of Macromolecular Chemistry, Academy of Sciences of the Czech Republic, Heyrovsky Sq. 2, 162 06 Prague 6, Czech Republic, donatork@gmail.com (R.K.D)*

[4] *MackGraphe - Graphene and Nanomaterials Research Center, Mackenzie University, Rua da Consolação 896, São Paulo 01302-907, Brazil, guilherminojmf@gmail.com (G.J.M.F.), ricardo.andrade@mackenzie.br (R.J.E.A.)*

[5] *Istituto per i Polimeri, Compositi e Biomateriali (IPCB), Consiglio Nazionale delle Ricerche (CNR), Via Campi Flegrei 34 Olivetti, 80078 Pozzuoli (NA), Italy, rosadimaio1988@libero.it (R.M.), clara.silvestre@ipcb.cnr.it (C.S.)*

*__Corresponding Authors:__ Radost Ivanova- e- mail: r.ivanova@imbm.bas.bg

Abstract

The surface properties of nanofillers and surface/interfacial interactions between fillers and matrix play crucial roles in the control of the properties of composites, especially considering hybrid materials used in biomedical, electronic and energy applications. In the present work, we investigate the surface properties of mono-filler and bi-filler composites of poly (lactic acid) (PLA) with graphene nanoplatelets (GNP) and multi-walled carbon nanotubes (MWCNTs) prepared by melt extrusion method. Zeta potential, contact angle (surface energy), Raman spectroscopy, and atomic force microscopy were used to evaluate the interaction between PLA matrix, GNP and MWCNTs particles, and also to characterize filler-polymer composite properties at the surfaces of the film. The effect of filler loading in the GNP/PLA and GNP/MWCNT/PLA composite films surface properties was investigated using surface Zeta potential by streaming and Contact angle measurements. The results suggest that the surface characteristics of the composite film may be synergistically tuned by incorporation of GNPs and MWCNTs with controlling the filler contents and filler combinations.

Keywords: Carbon nanotubes, Graphene nanoplates, Poly (lactic acid) polymer, Contact angle, Wettability, Surface roughness, Surface energy, Isoelectric point, Interfacial interaction, Raman analysis.

1. Introduction

Surfaces are inherently high-energy sites, and as nanofillers present high surface areas their surface energy is particularly high. When the nanofillers are added to a polymer matrix their surface energy may result in strong interfacial interactions with the polymer, which determine the improvement of nanocomposite properties [1]. The surface properties of nanofiller and polymer are particularly important to predict the dispersion of filler and interfacial interactions in polymer nanocomposites, however results focused on estimation of surface characteristics of the nanocomposites based on the surface characteristics of the fillers and its distribution in the polymer matrix are rarely reported, mainly when graphene and CNT are used. Moreover, surface properties of the final nanocomposites are important to be characterized, since they govern the compatibility of the nanocomposites with other surfaces (materials, microorganisms, cells, etc.), affecting properties and consequently applications, such as wettability/gas permeation in packaging, improved friction of materials for tribological application [2], cell adhesion in biocompatible materials [3] and microorganism proliferation in antimicrobial materials) [4], and etc. Especially concerning biomedical fields, most of the PLA applications in the biomedical field are supported by its intrinsic biosorption property, which are govern by wettability and surface energy. Therefore, a control of the surface properties by the insertion of carbonaceous nanofillers could contribute to improved biocompatibility and/or osteointegration, by tuning the hydrophobicity of the polymer with a controlled presence of nanofiller. Zeta potential is a physicochemical parameter of specific significance in portraying the surface electrical properties of charged media, and it is a useful parameter for determining electro-kinetic surface properties of both pristine and modified surfaces. The zeta potential can be determined by different electro-kinetic measurements such as streaming potential, electro–osmosis, sedimentation potential, electrophoresis and isoelectric point (IEP). The induced electrokinetic effect depends on driving force and the nature of solid and liquid phases [5]. Experimentally, the Zeta potential for a solid surface is

measured via a streaming potential, which occurs by forcing fluid through a channel. It is pH dependent due to the acid/base properties of the surfaces, and the pH at which the surface charge is zero is called the isoelectric point (IEP) and is typically used to quantify or define the electro-kinetic properties of a surface.

Analyte adsorption and charge transfer are interfacial processes that are very sensitive to the surface charge at the graphene-liquid interface and the capability tune the isoelectric point is hence fundamentally important [6]. However, the zeta potential of nanocomposites films of filler/ polymer is still poorly known because of the difficulty to interpret streaming potential experiments.

Moreover, the presence of graphene derivatives is known to affect the surface properties of polymer composites, particularly its wettability, e.g., the incorporation of small loadings of GNP are able to considerably change the surface wettability of PLA composite films [7] or when graphene oxide is used as filler for polyvinyl alcohol (PVA) to tune the surface properties of the nanocomposite [8]. Results of contact angle for carbon nanotubes (CNT) and different polymers, such as polypropylene (PP), polyethylene glycol (PEG), poly(methylmethacrylate) (PMMA), polyvinylidene fluoride (PVDF) are reported in the literature. Among the reported values, significant differences are observed for similar composite systems, making it difficult for a consistent conclusion.

Wettability measurements in co-operation with surface zeta potential by streaming measurements could provide a complementary approach to investigate the surface/interfacial properties of composite systems [9-13]. Wetting of nanofiller by surrounding polymer media is necessary in order to transfer the unique properties of the nanofiller to the matrix polymer. The interfacial interactions and the percolation threshold of nanofillers are determinant for the nanocomposite properties [14-16]. If the interface is weak, the composite has low strength and stiffness, but high resistance to fracture, while the strong interface interactions result in a brittle material with high strength [15]. Evolution of properties around the percolation

threshold of carbon nanotubes in polymer nanocomposites, related to the interfacial interactions was reported [14]. However, there is a need for further research in this area related to the effects of filler types and filler combinations.

Therefore, herein we report on surface properties characterization of poly (lactic acid) (PLA)-based nanocomposites incorporating graphene nanoplatelets (GNP) and mixed filler of GNP and multi-walled nanotubes (MWCNTs) with varying filler ratios. The effect of filler types and filler loading on surface properties of composite films were studied by measuring the isoelectric point and contact angle and calculating the surface free energy of composites films. The significance of this study is related with application of a new strategy to tune the surface properties of PLA matrix by concentration variation and combination of GNP and MWCNT fillers.

2. Experimental details

2.1. Materials

The poly(lactic) acid (PLA) polymer used in this study was Ingeo™ Biopolymer PLA-3D850 (Nature Works) with MFR 7-9 g/10 min (210°C, 2.16kg), peak melt temperature ~180 ºC, glass transition temperature ~ 60 °C. Ingeo™ 3D850 is a grade developed for manufacturing oϕ 3D printer filament. Graphene nanoplatelets (GNPs) adopted as nanofillers were supplied from Times Nano, China, having commercial code (TNGNP). Multiwall carbon nanotubes (MWCNTs) were purchased from Nanocyl S.A. (Belgium). In this study, we have used the Nanocyl 7000 series produced via the catalytic carbon vapor deposition process, without any further purification. The specific features of the used carbon nanofillers are collected in Table 1.

Table 1. Characteristics of GNPs and MWCNTs used in PLA nanocomposites

Characteristics	**GNPs**	**MWCNTs**

	(TNGNP)	(Nanocyl 7000)
Purity, wt.%	>99,5	>90
Number of layers / Thickness, nm	<20 / 4-20	-
Diameter/medium size, µm	5-10	-
Length, µm	-	1.5
Outer diameter, nm	-	9.5
Aspect ratio	500	~157
Transition Metal oxide, %	-	<1
Surface area, m^2/g	-	250-300
Volume resistivity, ohm.cm	4.10^{-4}	10^{-4}

2.2. Preparation of nanocomposites

Nanocomposites were prepared by melt extrusion at 170 – 180 ^{o}C, using a twin-screw extruder (COLLIN Teach-Line ZK25T) at screw speed of 40 rpm. Masterbaches of 9 wt% GNP/PLA and 9wt% MWCNT/PLA were initially prepared and further diluted with PLA by extrusion to produce mono-filler composites with varying filler contents from 1.5 to 9 wt.% GNP. The bi-filler composites (GNP/MWCNT/PLA) with 6 wt.% and 9 wt.% total filler content and GNP: MWCNT ratios of 1:1, 2:1, 3:1 and 5:1 were fabricated by mixing the composites 9 wt% GNP/PLA and 9 wt% MWCNT/PLA with neat PLA in appropriate amounts. Disk shape samples of diameter 1 cm and thickness 100 µm for surface Zeta potential measurements and square shape samples with size 2x2 cm and thickness 100 µm for Contact angle measurements were prepared by hot pressing.

2.3. Experimental methods

The surface zeta potentials were determined by streaming potential measurements that are surface sensitive [17]. Zeta potential (ξ) analysis was performed as a function of pH to

determine the isoelectric point (IEP). The isoelectric point of the flat surface of the neat PLA and nanocomposites with incorporating varying amounts of GNP and MWCNT in PLA matrix were measured at room temperature by SurPASS electrokinetic analyzer (Anton Paar GmbH, Austria). All measurements were conducted with an adjustable-gap cell The required pH value in the samples was adjusted by adding an appropriate amount of 0.05M HCl or 0.05M NaOH. The zeta potential measurements were carried out in the pH value range of 2 – 6. For each pH, the zeta potential measurement was repeated 4 times and the average value was taken.

Wetting experiments have played an important role for understanding of surface properties of graphene and its nanocomposites [18]. The contact angle measurement is one of the most popular methods used to quantify the wettability of the surface. The contact angle (CA) of the liquid droplet on the flat film surface was measured by using a DSA100 – KR*Ü*SS goniometer (Kruss, Hamburg, Germany) for two different liquids, Mili Q water and ethylene glycol, with varying surface tension at 20 °C to determinate the Surface Free Energy (SFE). Table 2 shows the surface free energy for the two liquids used in this study.

Table.2. Surface free energy of the liquids used in this study at 20°C in mJ/m^2

Liquids	Surface energy, [mJ/m^2]		
	γ	γ^d	γ^p
Mili Q water	72.8	21.8	51
Ethylene glycol	47.7	21.3	26.4

The used liquids were deposited onto the film by a sessile drop method [19]. The fitting used for each drop was determined from at least twenty measurements performed for each sample. An image of the drop is recorded with a camera and transferred to the drop shape analysis software. Data were collected with Advance Drop shape software, from *KRÜSS*. The program performs a contour recognition based on the grey-scale analysis of the image. The

data is then fitted to a geometrical model to the contour. Ellipse calculation method [20] was chosen to calculate the contact angle during these measurements. All measurements were made in static contact angle mode.

The surface energy (γ) values were calculated using Owens, Wendt, and Kaelble's method [21,22].

The values of the contact angles (water and ethylene glycol) were used to calculate the surface energy (γ) using the following equation [23]:

$$\gamma_s = \gamma_s^d + \gamma_s^p \quad (1)$$

where γ_s is the SFE, γ_s^d is the dispersion component of SFE and γ_s^p is the polar component of SFE.

Components γ_s^d and γ_s^p of the examined materials may be calculated from:

$$(\gamma_s^d)^{0.5} = \frac{\gamma_{EG}(cos\theta_{EG}+1) - \sqrt{\left(\frac{\gamma_{EG}^p}{\gamma_w^p}\right)}\gamma_w(cos\theta_w+1)}{2\left(\sqrt{\gamma_{EG}^d} - \sqrt{\gamma_{EG}^p\left(\frac{\gamma_w^p}{\gamma_w^p}\right)}\right)} \quad (2)$$

$$\left(\gamma_s^p\right)^{0.5} = \frac{\gamma_w(cos\theta_{EG}+1) - 2\sqrt{\gamma_s^d\gamma_w^d}}{2\sqrt{\gamma_w^p}} \quad (3)$$

where γ_s^d is the dispersive component of SFE of the examined materials, γ_s^p is the polar component of SFE of the materials examined, γ_{EG} is the free SFE of ethylene glycol, γ_{EG}^d is the dispersive component of ethylene glycol surface energy, γ_d^p is the polar component of ethylene glycol SFE, γ_w is the SFE of water, γ_w^d is the dispersive component of water SFE, γ_w^p is the polar component of water SFE, θ_d is the contact angle of ethylene glycol and θ_w is the contact angle of water.

The polar component is the sum of polar, hydrogen, inductive, and acid-base interactions, while the dispersive component accounts for van der Waals and other non-site-specific interactions [24-26].

Raman spectroscopy analyses of PLA/ GNP and PLA/ GNP/ MWCNTs films were performed on a microscope coupled to a spectroscope Raman scattering, Witec UHTS 300, using a 532 nm laser with 1.5 mW power intensity at the following conditions: filler single spectra, magnificatin: 50x, integration time 0.5 s; 532 nm excitation laser at room temperature. The system with its Raman capability combines a highly efficient Raman spectrometer with a high resolution confocal optical microscope. Pressed film samples with thicknesses of about 0.1 mm were tested. Band fitting was performed using Origin Pro software.

For analysis of the structure, morphology and surface roughness, the bright field transmission electron microscopy (TEM) analysis and the atomic force microscopy (AFM) were performed. The FEI TECNAI G12 Spirit-Twin (LaB6 source) TEM instrument was equipped with a FEI Eagle-4k CCD camera and operating with an acceleration voltage of 120 kV. The analysis was performed on sections obtained at room temperature by using a Leica EM UC6/FC6 ultra-microtome. The sections were placed on 400 mesh copper grids. The AFM analysis was performed using QScopeTM 250/400 instrument.

3. Results and discussion

3.1. Mono-filler GNP/PLA composites

3.1.1. Zeta potential measurements

The investigation of surface energy of graphene and carbon nanotube – based composites interface is of great importance because it is strongly influenced by the wettability of those nanofillers from the matrix polymer [26, 27]. The surface properties of the PLA-based nanocomposites, as varying the filler types and contents were evaluated by zeta potential

measurements. Figure 1 presents zeta potential curves as a function of pH for mono-filler GNP/PLA nanocomposites with varying GNP content, compared to the neat PLA.

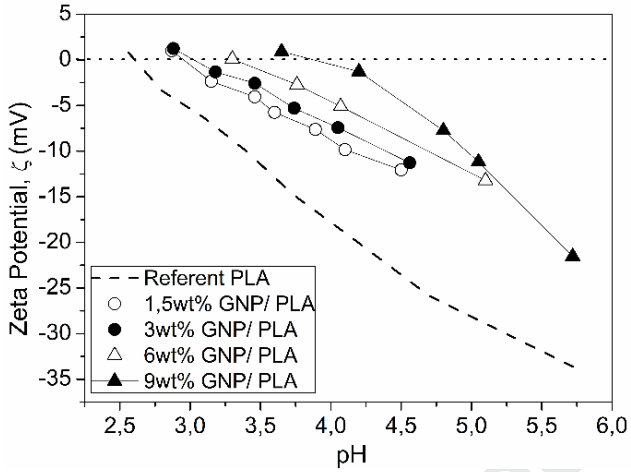

Fig.1. Zeta potential versus pH factor of mono-filler, GNP/PLA composites, as varying the graphene content.

The isoelectric point (IEP), that is the pH at zero zeta potential of the films, was observed at pH = 2.6 for the neat PLA, and it increases gradually to pH=3.6 by increasing the GNP content from 1.5 to 9 wt.%. The values of measured IEP and zeta potential |ζ| for GNP/PLA composites are summarized in Table 3.

Table 3. Isoelectric point (IEP) and zeta potential |ζ|) of mono-filler GNP/PLA composites with varying GNP contents from 0 to 9 wt%.

Sample	Isoelectric point [pH]	Zeta potential limits, |ζ|, mV
Neat PLA	2.5	1.7 to -33.59
1.5wt%GNP/ PLA	2.9	1 to -12.06
3wt%GNP/ PLA	2.9	1.24 to -11.28

6wt%GNP/ PLA	3.3	0 to -13.22
9wt%GNP/ PLA	3.7	0.9 to -21.53

Above 6 wt% GNP content, the increases of both IEP and Zeta potential become stronger compared to that at lower filler contents. This may be associated with particle-particle interactions, which obviously dominate over polymer–particle interactions and lead to formation of a percolated network of interconnected graphene platelets in the hydrophilic PLA polymer. Percolation occurs when there are enough particles to form a consistent network by physical contact of electrons through thin layers of matrix separating the inclusions. As the graphene amount in GNP/PLA composite increases, the fillers particles form a continuous path for dissipation of energy (electrons transfer) through the volume of the sample. Therefore, the increase of the absolute values of Zeta potential from 13 to 22 mV above 6 wt% GNP, as well as the increase of the IEP from pH 2.6 for PLA to 3.6 for 9 wt% GNP/ PLA may be associated with electrical percolation due to the formation of spatial structure of conductive graphene platelets in the polymer matrix, which facilitates the electron transfer. Our previous studies on rheological behavior [28, 29] and electrical properties [29] of the same GNP/PLA composites also pointed that the percolation appears above 6 wt% graphene content.

3.1.2. Contact angle measurements

Contact angle measurements investigate wettability and surface tension, and they are used to calculate the surface free energy (SFE) of the films, incorporating graphene and carbon nanotubes [30, 31]. Contact angle data for the two test liquids (water and ethylene glycol) applied for the mono-filler system GNP/PLA are plotted in Figure 2. Calculated Surface free energy and its polar and dispersive components are presented in Figure 3. The average values

of all surface characteristics for the mono-filler GNP/PLA composites are summarized in Table 4.

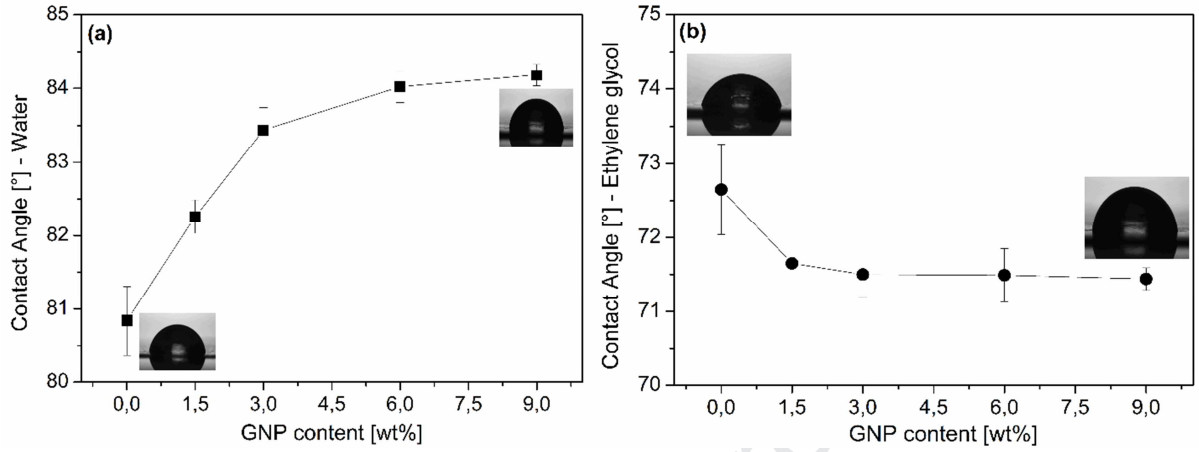

Fig.2. Contact angle vs. GNP content for mono-filler GNP/PLA composite for the two test liquids: (a) water; (b) ethylene glycol.

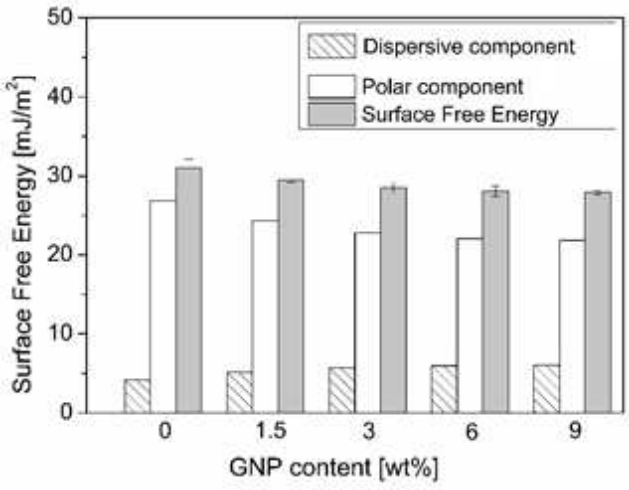

Fig.3. Calculated surface free energy and its dispersive and polar components vs. filler content for the mono-filler GNP/PLA composites.

Table 4. Contact angle for two liquids (at 20°C) and surface energy components of mono-filler GNP/PLA composites.

Sample	Contact Angle, [°]		Surface energy, [mJ/m^2]		
	Mili Q water	Ethylene glycol	γ_s	γ_s^d	γ_s^p

Neat PLA	80.8±0.5	72.6±0.6	31.1±1.1	4.2	26.9
1.5wt%GNP/ PLA	82.3±0.2	71.6±0.1	29.5±0.4	5.2	24.3
3wt%GNP/ PLA	83.4±0.3	71.5±0.3	28.5±0.6	5.7	22.8
6wt%GNP/ PLA	84.0±0.2	71.5±0.6	28.1±0.6	6.0	22.1
9wt%GNP/ PLA	84.2±0.1	71.4±0.1	27.9±0.3	6.0	21.9

It can be observed that with increasing the GNP content to 6 wt% and 9 wt%, slightly higher water droplet contact angle values (84^o) are obtained, in comparison with the neat PLA (81^o). This may be associated with a hydrophobic contribution of the GNP filler, around and above the percolation threshold. In agreement with the literature, the composites obtained in our study present contact angle values near to the upper hydrophilicity limit of $0° < \theta < 90°$ [32, 33], corresponding to a moderate wettability that decreases with the addition of GNPs.

The contact angle values for ethylene glycol were about 10^o lower than that of water. The θ values slightly decrease (from 73° to 71°) with the addition of only 1.5% GNP, but it reaches a plateau with further increasing the GNP content to 9 wt.%. Results show that the wettability of GNP/PLA composite surfaces to organic liquids is much higher than this to water.

The two different liquids (water and ethylene glycol), with known polar and disperse components (Table 2), were used to calculate the surface free energy from the contact angle measurements of the PLA and the composite films. The variation of the surface free energy against the filler contents is given in the Figure 3, showing γ_s (surface energy) and its polar (γ_s^p) and dispersive (γ_s^d) component of the mono-filler GNP/PLA composite, compared to the neat PLA. Looking at the data (Fig. 3 and Table 4), we can note that there is a small gradual decrease of the surface energy (γ_s), by increasing the GNP content. The decrease in γ is mainly caused by a slight reduction in the polar component, which involves a strongly polarized interaction of hydrogen bonds, indicating for less polar groups at the surface of the

film. This may be associated with a slight increase of the interfacial polymer-filler interactions, by increasing the GNP content. On the other hand, the dispersive component, which corresponds to the Van der Waals forces, is slightly increasing, which indicates a small increase in particle-particle interactions with increasing the GNP content.

3.2. Bi-filler GNP/MWCNT/PLA composites

3.2.1. Zeta potential measurements

Figure 4 presents the zeta potential curves as a function of pH for bi-filler GNP/MWCNT/PLA nanocomposite films with 6 wt.% (Fig.4a) and 9wt.% (Fig.4b) total filler content, with varying the GNP: MWCNT fillers ratio of 1:1, 2:1, 3:1 and 5:1. Table 5 summarizes the IEP and |ζ| values for the bi-filler composites compared to the mono-filler ones with the same total filler content.

In general, the addition of small amounts of 1.5% MWCNTs as a secondary filler to GNP decreases significantly the IEP values and increases the absolute Zeta potential values, when compared to the mono-filler GNP/PLA composites with the same total filler content.

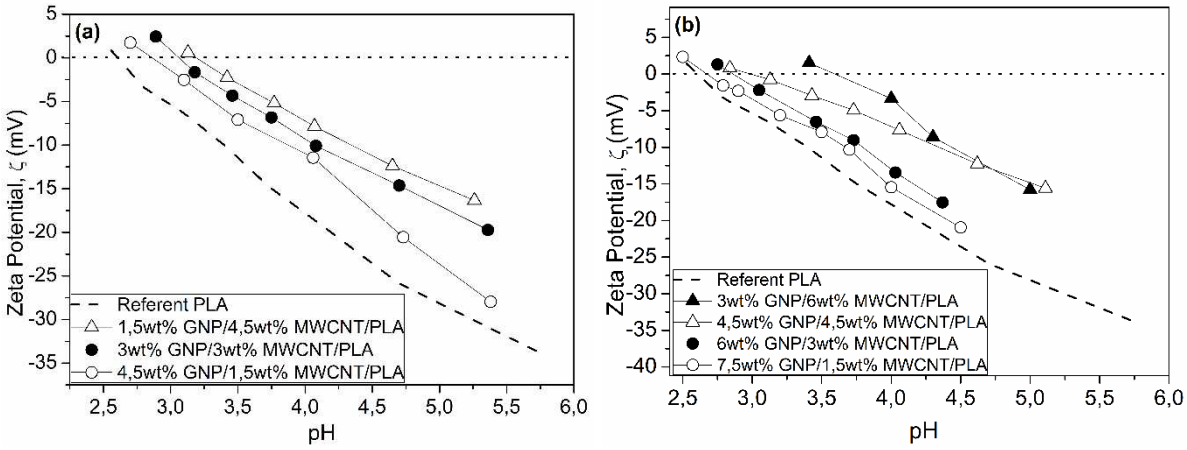

Fig.4. Zeta potential in function of the pH for the GNP/MWCNT/PLA composites, as varying the filler ratios (with increasing of MWCNTs), at total amount of filler: (a) 6wt% and (b) 9wt%.

With increasing the amount of MWCNTs and decreasing, respectively, the amount of GNPs in the 6wt% and 9wt% GNP/MWCNT/PLA bi-filler composites, the IEP increases gradually due to the electron cloud that makes the nanotubes negatively charged, while the |ζ| values increase. In our previous study [29], the percolation threshold was observed below 3 wt% filler content in those bi-filler composites, therefore, the percolated network is definitely formed in the 6wt% and 9wt% GNP/MWCNT/PLA bi-filler composites.

It worth noting that for these measurements, PLA was used only as a guideline for comparison with the nanocomposites, since; in theory the zeta potential values of the neat PLA and the nanocomposites are not comparable due to the dominant filler effect. This is mainly due to the measuring cells of (solid) surface zeta potential that receive a liquid flow through, producing a pressure gradient and a charge separation at the solid/liquid interface, where the streaming potential is the electrical response to the shift in the surface charge. Consequently, two main factors influence the outcome; i) the native surface charge, which in the case of a non-conductive polymer like PLA is mostly derived from its chemical structure composed of available electron pairs from both oxygens of the ester group formed (a non-ionogenic group); and ii) the variation of the material's conductivity (only for nanocomposites), since the increased electron availability at the material surface creates a negative potential. Altogether, the electron-rich non-ionogenic groups from PLA drag the zeta potential down and only at quite low pH the IEP is reached. However, the addition of the (also electron-rich) fillers changes the availability of these groups and increases the repulsion forces, decreasing the zeta potential. At this point, the filler effect on the zeta potential becomes dominant, and the increase of electron conductivity produces the main variation of isoelectrical point and zeta potential range.

Table 5. Isoelectric point (IEP) and zeta potential |ζ|) of the bi-filler GNP/MWCNT/PLA composites with varying filler ratios, compared to the mono-filler GNP/PLA composites of 6 and 9 wt% filler.

Sample	Isoelectric point [pH]	Zeta potential limits |ζ|, mV
Pure PLA	2.5	1.7 to -33.59
6% GNP/PLA	3.3	0 to -13.22
4.5wt% GNP/ 1.5wt%MWCNT/ PLA	2.7	1.7 to -27.96
3wt% GNP/ 3wt%MWCNT/ PLA	2.9	2.4 to -19.72
1.5wt% GNP/ 4.5wt%MWCNT/ PLA	3.1	0.6 to -16.34
9% GNP/PLA	3.7	0.9 to -21.53
7.5wt%GNP/ 1.5wt%MWCNT/ PLA	2.5	2.3 to -20.95
6wt%GNP/ 3wt%MWCNT/ PLA	2.75	1.3 to -17.52
4.5wt%GNP/ 4.5wt%MWCNT/ PLA	2.8	0.8 to -15.59
3wt%GNP/ 6wt%MWCNT/ PLA	3.4	1.53 to -15.78

3.1.2. Contact angle measurements

The water and ethylene glycol contact angle data obtained from the bi-filler system of 6wt% GNP/ MWCNT/ PLA are plotted in Fig. 5, and the calculated Surface free energy and its polar and dispersive components are presented on Fig. 6. The average values of all surface properties for the bi-filler systems are summarized in Table 6.

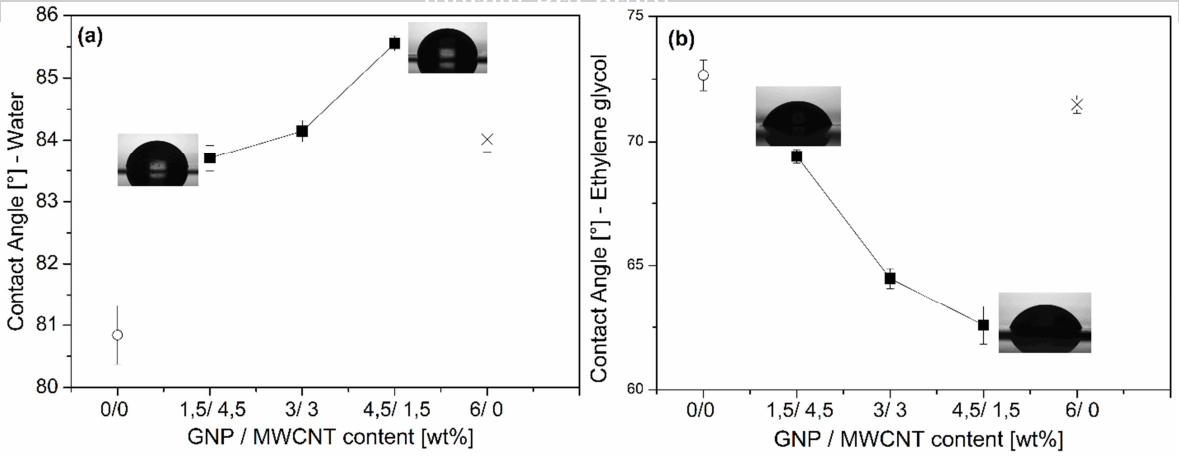

Fig.5. Contact angle in function of GNP/MWCNT ratio in bi-filler composite at 6 wt% GNP/MWCNT/PLA, for the two test liquids: (a) water; (b) ethylene glycol. The single end points refer the neat PLA and the mono-filler GNP/PLA composite.

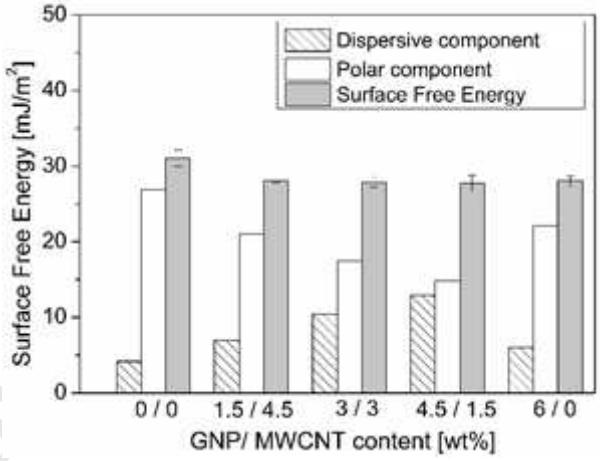

Fig.6. Calculated surface free energy from contact angle results for 6 wt% GNP/MWCNT/PLA bi-filler composites, with varying the filler ratio, compared to PLA and 6wt% GNP/PLA.

Table 6. The contact angle (at 20°C) and surface energy components of bi-filler composites, GNP/MWCNT/PLA.

Sample	Contact Angle, [°]		Surface energy, [mJ/m^2]		
	Mili Q water	Ethylene glycol	γ_s	γ_s^d	γ_s^p
Neat PLA	80.84±0.47	72.65±0.61	31.05±1.07	4.17	26.88

6wt%GNP/ PLA	84.0±0.2	71.5±0.6	28.1±0.6	6.0	22.1
4.5wt%GNP/ 1.5wt% MWCNT/ PLA	85.55±0.12	62.58±0.75	27.77±1.05	12.9	14.87
3wt%GNP/3wt% MWCNT/PLA	84.15±0.17	64.48±0.4	27.88±0.64	10.41	17.47
1.5wt%GNP/ 4.5wt% MWCNT/ PLA	83.71±0.21	69.4±0.29	28.04±0.21	7.01	21.03
9wt%GNP/ PLA	84.2±0.1	71.4±0.1	27.9±0.30	6.0	21.9
7.5wt%GNP/1.5wt% MWCNT/ PLA	86.23±0.41	64,97±0,15	26,97±0,78	11,51	15,47
6wt%GNP/ 3wt% MWCNT/ PLA	85.6±0.08	65,02±0,03	27,18±0,14	11	16,18
4.5wt%GNP/4.5wt% MWCNT/ PLA	84.91±0.24	67,17±0,49	27,26±0,77	9,04	18,22
3wt%GNP/ 6wt% MWCNT/ PLA	83.97±0.04	68,42±0,15	27,8±0,2	7,72	20,08

The bi-filler composites seem to present the same tendency, as the previous results with the mono-filler ones. The water contact angle of 6wt% GNP/MWCNT/PLA film increased about 5°, comparing to the pristine PLA films, showing a higher hydrophobic effect. The water droplet rests on the surface of bi-filler composites and spreads to form a contact angle that indicate wettability by water with moderate hydrophilic characteristics [33] (Fig. 5a). The static aqueous contact angle values (84-86°) suggested that the GNP/MWCNT/PLA nanocomposites have slightly lower wettability compared to that of the neat PLA (81°). The lowest water wettability was observed for the bi-filler composites with the highest MWCNT content.

Importantly, the contact angle of ethylene glycol liquid drastically decreases (to 63°) by adding a small amount of 1.5% MWCNTs as a secondary filler compared to the mono-filler GNP/PLA composites (72°), at the same total filler content. However, further increase of the MWCNTs amount in the bi-filler composites, leads to an increase of the contact angle values to about 69° (Fig. 5b). The results confirm much better wettability of bi-filler composites by the organic liquid, compared to the neat PLA and the mono-filler one at the same filer content.

The variation of surface free energy against the filler ratios for the bi-filler 6wt% GNP/MWCNT/PLA composite is given in the Fig. 6, which shows surface energy (γ_s) and its polar (γ_s^p) and dispersive (γ_s^d) component. Results for the bi-filler composites are compared to that of neat PLA and the mono-filler 6wt% GNP/PLA. One can see that the surface energy of the bi-filler composites is insufficiently changed with varying the filler ratio, however, adding a small amount of 1.5% MWCNTs as a secondary filler produce a strong increase of the dispersive component and a respective decrease of the polar components, compared to the mono-filler one.

These findings are confirmed for the bi-filler composites at 9 wt% total filler contents. Contact angle data for the two test liquids are plotted in Fig. 7, and average values are shown in Table 6. The water contact angle of 9 wt% GNP/MWCNT/PLA film increase of about 6◦ and the ethylene glycol contact angle decreased about 8°, comparing to the pristine PLA film, similar to the values obtained for the 6 wt% bi-filler systems.

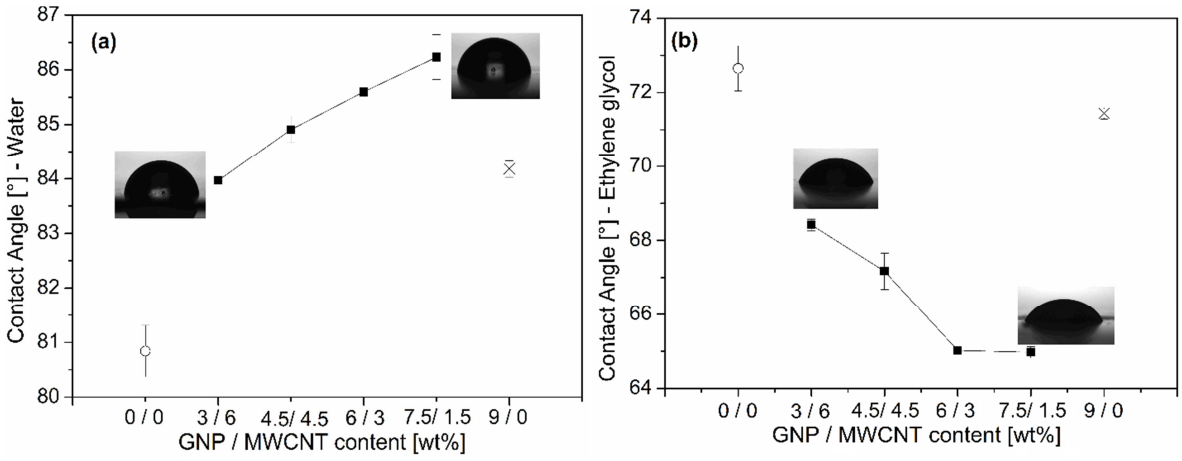

Fig.7. Contact angle in function of GNP/MWCNT ratio for bi-filler composites with 9 wt% filler content, for the two test liquids: (a) water; (b) ethylene glycol. The single end points refer the neat PLA and the mono-filler GNP/PLA composite.

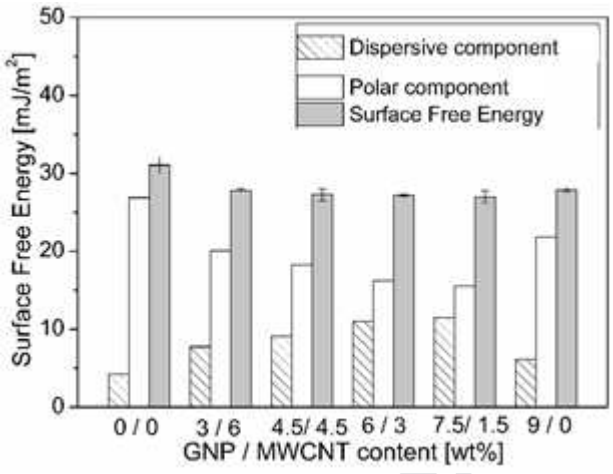

Fig.8. Calculated surface free energy from contact angle data for bi-filler 9 wt% GNP/MWCNT/PLA composites, as varying the filler ratio, compared to neat PLA and 9wt% GNP/PLA.

The variation of surface free energy against filler's content for the 9 wt% bi-filler composites is given in the Fig. 8, which shows the surface energy (γ_s) and its polar (γ_s^p) and dispersive (γ_s^d) component. Results are compared with the neat PLA and mono-filler 9wt% GNP/PLA (the single end points). The changes in surface energy (γ_s) were not so significant, however, the addition of small amount of 1.5% MWCNTs in the bi-filler composites caused about 2-folds reduction in the polar component. This indicates the formation of a strongly polarized interaction of hydrogen bonds, between PLA and the two fillers, and that less polar groups are available at the surface of the film. Therefore, stronger interfacial and inter-particle interactions are obtained in the bi-filler composites GNP/MWCNT/PLA, compared to the mono-filler systems GNP/PLA. In contrast, the dispersive component increases twice in the bi-filler systems with the smallest MWCNT contents (1.5-3 wt%), which may be associated with a stronger interconnection of GNP and MWCNT particles.

3.3. Raman spectroscopy

With the intention to prove our findings**,** Raman spectra were used to evaluate the interaction between PLA and, GNP and MWCNTs particles. The Raman spectra of the graphene nanoplates (GNP) as a powder and after extrusion to PLA/GNP nanocomposites are shown in Fig.9.

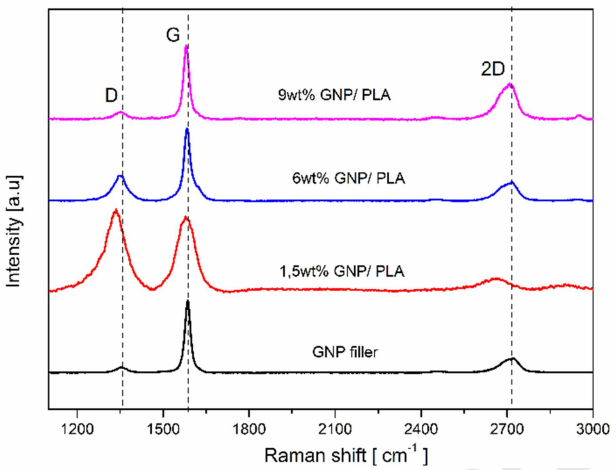

Fig.9. Normalized Raman spectra of mono-filler – PLA/ GNP composite (pressed films), as varying the filler contents.

The GNPs were identified by the positions of the G, D and 2D bands, as well as the ratios of intensities between bands D and G (I_D/I_G) and 2D and G (I_{2D}/I_G), which are summarized in Table 7 for the different amounts of GNP in PLA matrix. The intensity ratios (I_D/I_G) values are often used to estimate the number of defects and aproximated number of layers in carbon materials. For one to four-layer graphene sheets, this ratio decreases with increasing the amount of filler. This can be understood as indicating the recovery of damaged graphene at higher amount of filler. The observation of the D bands increase indicated that defects were introduced into the graphene in nanocomposites after extrusion. This may be caused by damage to the filler during extrusion, or by the interaction between PLA and graphene. Our results show that the extrusion methods had a significant effect on the number of defects. The D band was considerably increased at low concentration of 1.5 wt.% GNP (highest D band).

With increasing of the amount of GNP filler to 9wt%, the D band intensity decreased, therefore the defects were considerably decreased.

Compared to the Raman spectra of the neat GNP filler, the Raman spectra of GNP/ PLA showed an obvious shift to lower values (redshift). The strong G band redshift could be an indication of stress effect caused by the strong interaction between GNP and PLA matrix. In general, the position of G and 2D bands in the composites was shifted to higher values by increasing the filler contents, namely: the positions of G and 2D bands were, respectively; 1588 cm^{-1} and 2663 cm^{-1} for 1.5wt%GNP/ PLA; 1578 cm^{-1} and 2700 cm^{-1} for 6wt%GNP/ PLA; and 1581 cm^{-1} and 2708 cm^{-1} for 9wt%GNP/ PLA. The 2D band, which is a second order D band, also differed in band position and shape, where a more intense and sharper 2D band represents few layers' graphene. As the number of layers increased, the 2D band is shifted to lower wavenumbers (Fig. 9), this indicating that by increasing the filler content in the GNP/PLA composites, the number of layers in GNP increased due to the worsen dispersion of nanofiller in the PLA matrix by extrusion.

The position of the D band, G band and 2D band for the bi-filler composites are summarized in Figure 10 and Table 7.

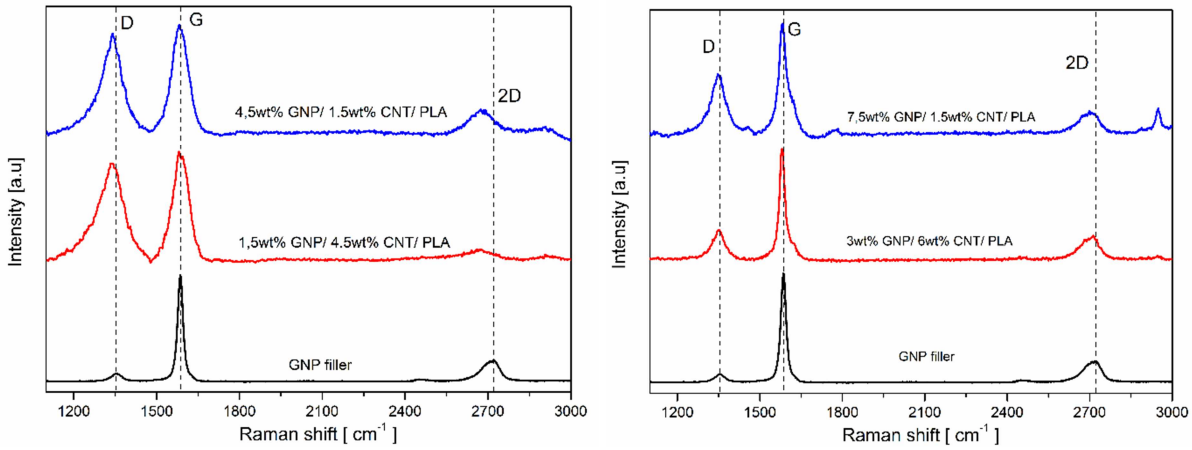

(a) (b)

Fig.10. Normalized Raman spectra of the bi-filler PLA/ GNP/ MWCNT composite films, as varying the filler combinations and total amount of 6wt.% (a) and 9wt.% (b) filler contents.

For the bi-filler composites (GNP/ MWCNT/ PLA) with increasing amount of fillers, a D band intensity decrease was observed, which is related to defects in structure. Our observation indicates that the interaction between fillers and polymer matrix is not strong enough to affect the physical structure of fillers. Comparing the bi-filler composites, the formulations with 4.5wt% GNP/ 1.5wt% CNT/ PLA and 7.5wt% GNP/ 1.5wt% CNT/ PLA presented the lowest I_D/I_G ratio, i.e. less structural defects. Moreover, considering the I_{2D}/I_G ratios, all the systems presented only few layers (less than 10 layers) graphene dispersed in PLA matrix.

Table 7. Data from Raman characterization of nanocomposites in form of pressed films.

Sample in form of pressed films	D band Position cm^{-1}	G band Position cm^{-1}	2D band Position cm^{-1}	D Intensity	G Intensity	2D Intensity	I_D/I_G	I_{2D}/I_G
1.5wt% GNP/ PLA	1339	1588	2663	137.56	100	30.66	1.38	0.31
6wt% GNP/ PLA	1357	1578	2700	33.87	100	25.60	0.34	0.26
9wt% GNP/ PLA	1357	1581	2708	9.68	100	47.80	0.10	0.50
1.5wt% GNP/ 4.5wt% CNT/ PLA	1339	1583	2692	89.12	100	9.25	0.89	0.09
3wt% GNP/ 6wt% CNT/ PLA	1354	1583	2714	26.53	100	21.26	0.27	0.21
4.5wt% GNP/ 1.5wt% CNT/ PLA	1354	1583	2719	91.90	100	20.05	0.92	0.20
7.5wt% GNP/ 1.5wt% CNT/ PLA	1349	1586	2708	54.05	100	20.59	0.54	0.21
GNP filler	1359	1586	2723	7.19	100	19.40	0.08	0.12

CNT filler	1341	1580	2684	128.00	100	24.30	1.28	0.24

3.4. Microstructure of nanocomposites

With the intention to prove our findings, different visualization techniques were applied in order to identify incorporating the fillers to the polymer matrix and to verify the morphology and surface roughness of the surface of investigated films. The morphology of the mono-filler and bi-filler composites was visualized using transmission electron microscopy. Figure 11 presents the TEM micrographs of 9 wt% mono-filler GNP/PLA and bi-filler GNP/MWCNT/PLA systems with varying the ratio of fillers. In the 9 wt% GNP/PLA composite (Fig. 11a), the GNPs are visible as large agglomerates of a micron length. When a small amount of 1.5 wt% MWCNTs was added (Fig. 11b), few single nanoplatelets are visible, which attract the MWCNTs, but most of the GNPs remain in large agglomerates. The best exfoliation of GNPs and finest dispersion of MWCNTs is achieved in the bi-filler composite 6%GNP/3%MWCNT/PLA, having twice higher GNP content than MWCNTs (ratio 2:1) (Fig 11c). While, at equal ratio 4.5 wt% GNP/ 4.5 wt% MWCNT/PLA (Fig. 11d), as well as at higher amount of MWCNTs than GNPs (not presented here), a homogeneous dispersion of the MWCNTs is visible, hiding the GNPs. From TEM images it could be concluded that by increasing the MWCNTs content in the bi-filler composites, better dispersion and higher inter-particle interactions between the two anisotropic fillers were achieved. Thus, the addition of MWCNTs as a secondary filler to GNPs, in proportions 2:1 and 1:1 (GNP: MWCNT), built up a hybrid structure of well dispersed and interpenetrated nanofiller particles, which are percolated and form a conductive network in the insulating polymer matrix.

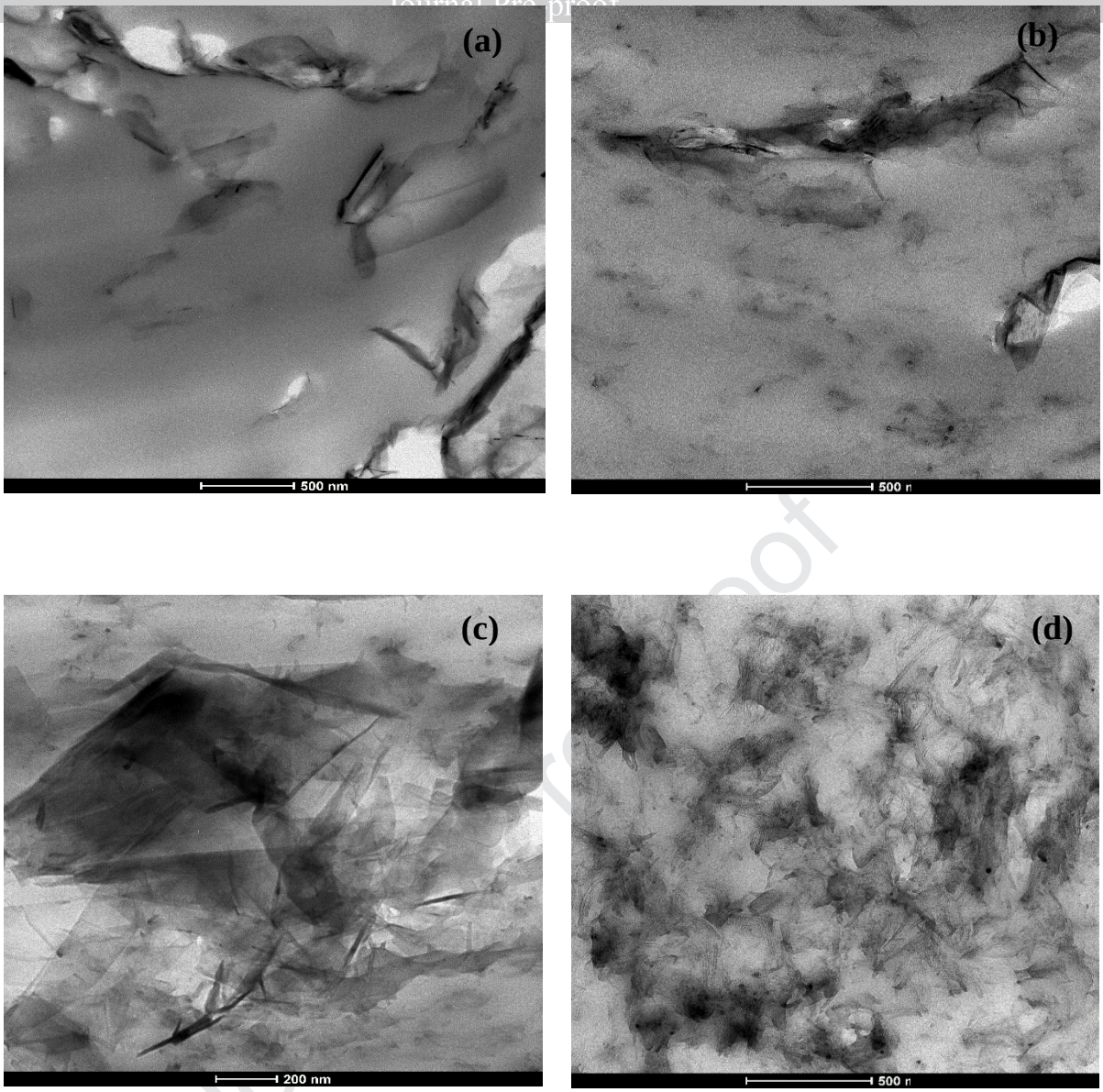

Fig.11. TEM micrographs of 9wt% mono-filler and bi-filler systems with different ratio of GNPs and MWCNTs: (a) 9wt% GNP/PLA; (b) 7.5wt%GNP/1.5wt%MWCNT/PLA; (c) 6wt% GNP/3wt%MWCNT/PLA; (d) 4.5wt%GNP/4.5wt%MWCNT/PLA.

AFM images were recorded on different zones in wave mode in order to be representative for the total sample surface topography. The surface roughness of the neat PLA, 6wt% GNP/PLA, 3wt% GNP/3wt% MWCNT/PLA and 4.5wt% GNP/1.5wt% MWCNT/PLA was verified by statistical AFM estimations. The average roughness (Sa) and standard deviation

have been calculated. Sa is the average deviation from the mean surface plane. The average values of all measured systems are summarized in Table 8.

Table 8. The average roughness and standard deviation of measured composites: neat PLA, GNP/PLA and GNP/MWCNT/PLA

Samples	**Sa (Average Roughness), nm**	**Standart Deviation, %**
Neat PLA	577.4	208.03
6wt% GNP/PLA	530.57	47.32
3wt% GNP/3wt% MWCNT/PLA	414.40	12.44
4.5wt% GNP/1.5wt% MWCNT/PLA	410.27	130.28

In Figure 12 the AFM 3D images and line profiles recorded for neat PLA and 6wt% GNP/PLA surfaces. The surface topography of PLA changes after additions of GNP fillers and new surface features are revealed.

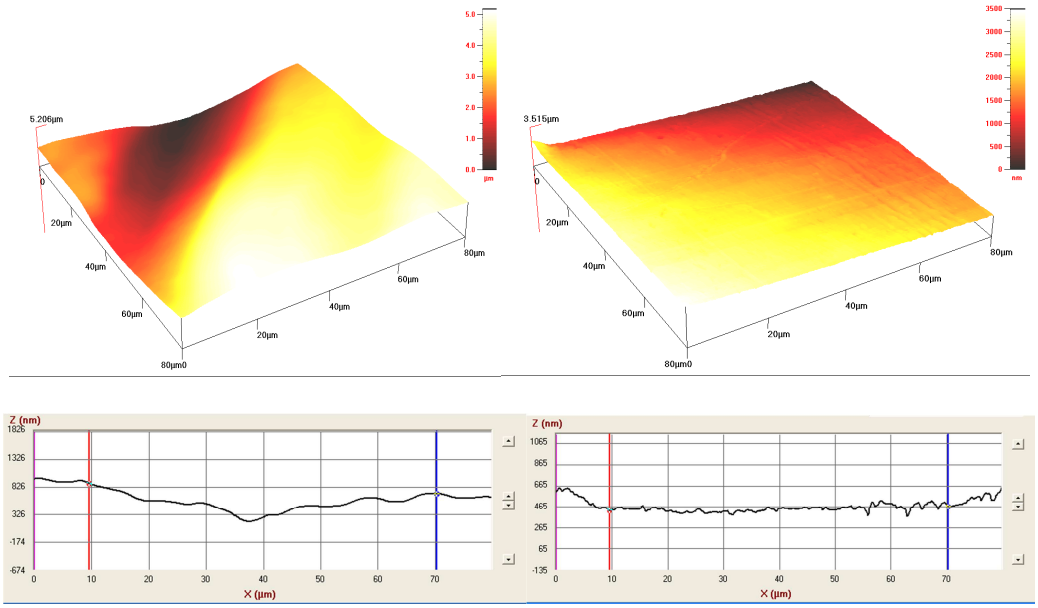

(a) (b)

Fig.12. Example AFM 3D images and line profiles recorded for neat PLA (a) and 6wt% GNP/PLA (b) surfaces.

It is evident from Table 8, that the bi-filler GNP/MWCNT film surface is much more smooth than the reference PLA and the mono-filler GNP/PLA surfaces if compare the AFM roughness. The neat PLA surface showed the highest average roughness (Sa) and a relatively high standard deviation. By incorporating the GNPs, the roughness of the mono-filler composite films decreases by 9%, compared to the neat PLA. While, the incorporation of the second filler MWCNTs, the average roughness decreases by around 29%, compared to the neat PLA. This can be associated with better dispersed and more homogenous GNP/MWCNT/PLA nanocomposites compared to the GNP/PLA mono-filler systems.

4. Conclusions

Measurements of zeta potential and contact angle were used to evaluate the polymer nanocomposite surface energy of the films. Enhancement of the surface properties of PLA nanocomposites by adding of GNP and MWCNT additives was achieved.

With increasing the GNP content above 6 wt%, the isoelectric point and zeta potential values increased, due to the formation of a percolated network of conductive graphene nanoplatelets. Concerning the bi-filler composites, with increasing the amount of MWCNTs and decreasing, respectively, the amount of GNPs, the IEP increases gradually, while the zeta potential values decrease, which is associated with a better dispersion and some stronger inter-particle interactions in the hybrid composites with higher MWCNT contents.

The surface free energy of the films could be successfully tuned by controlled incorporation of GNP and mixed GNP/MWCNT fillers. The increasing of GNP content in both mono-filler and bi-filler composites leads to a decrease of polar component, while the

dispersive component increases. The results are explained with increased interfacial polymer-filler interactions, as well as enhanced particle-particle interactions by controlling the GNP/MWCNT ratios.

The structure of nanocomposites visualized by TEM micrographs confirmed that the bi-filler composites GNP/MWCNT/PLA have much better dispersion and inter-particle interaction, rather than the mono-filler GNP/PLA, but this is strongly dependent on the filler ratios. The best GNP exfoliations and the finest MWCNT dispersions were obtained for the systems with GNP: MWCNT ratios of 2:1, 1:1 and 1:2. If compare the AFM roughness, the bi-filler GNP/MWCNT film surface is much more smooth than the reference PLA and the mono-filler GNP/PLA surfaces, this associated with better dispersed and more homogenous bi-filler GNP/MWCNT/PLA nanocomposites compared with the mono-filler GNP/PLA systems.

By increasing the filler content in the mono-filler GNP/PLA composites, the number of layers in GNP increased, as determined by Raman analysis, whuch is associated with the worsen dispersion in the PLA matrix. For the bi-filler composites, the 3:1 and 5:1 GNP/MWCNT formulation show less defects in the structure.

The obtained results can find various technological applications in controllable tuning of the surface properties of PLA based nanocomposite films by varying the filler contents and suitable combinations of graphene and carbon nanotubes.

ACKNOWLEDGMENTS

This work was carried out within the framework of the H2020-MSCA-RISE-2016-734164 Graphene 3D project. The research was partially supported by the Bulgarian Ministry of Education and Science under the National Research Programme “Young scientists and postdoctoral students” approved by DCM # 577 / 17.08.2018. R.I., R.K and E.I. acknowledged the support from H2020-SGA-FET-GRAPHENE-2017-785219 Graphene

Core2. RKD, GJMF and RJEA acknowledge the financial support of MackPesquisa (Project number 181009). This study was also supported in part by the Coordenação de Aperfeiçoamento de Pessoal de Nível Superior - Brazil (CAPES) - PRINT 88887.310339/2018-00. Authors thank Dr. V. Georgiev for the help in processing of nanocomposite materials.

REFERENCES

[1] J. Karger-Kocsis, H. Mahmood, A. Pegoretti, Recent advances in fiber/matrix interphase engineering for polymer composites. Prog. Mater. Sci. **2015,** 73, 1–43, DOI:10.1016/j.pmatsci.2015.02.003.

[2] D. H. Buckley, Tribological properties of surfaces, Thin Solid Films 1978, 53(3): 271–283

[3] M. Ferrari, F. Cirisano, M.C. Morá, Mammalian Cell Behavior on Hydrophobic Substrates: Influence of Surface Properties. Colloids and Interfaces. 2019; 3(2):48, doi.org/10.3390/colloids3020048

[4] S. Rigo, C. Cai, G. Gunkel□Grabole, L. Maurizi, X. Zhang, J. Xu, C. G. Palivan, Nanoscience□Based Strategies to Engineer Antimicrobial Surfaces, Adv.Sci. 2018, 5, 1700892, DOI: 10.1002/advs.201700892.

[5] M. Elimelech, W. H. Chen, and J. J. Waypa, Measuring the zeta (electrokinetic) potential of reverse osmosic membranes by a streaming potential analyzer. Desalination **1994**, 95(3), 269-286.

[6] S. Schauermann, N. Nilius, S. Shaikhutdinov, H. J. Freund, Nanoparticles for heterogeneous catalysis: New mechanistic insights. Acc. Chem. Res. **2013**, 46, 1673–1681, doi: 10.1021/ar300225s.

[7] A. M. Pinto, S. Moreira, I. C. Gonçalves, F. M. Gama, A. M. Mendes, F. D. Magalhaes, Biocompatibility of poly (lactic acid) with incorporated graphene-based materials. Colloids Surf B Biointerfaces **2013**, 104, 229–238, doi: 10.1016/j.colsurfb.2012.12.006.

[8] C. F. P. De Oliveira, P. A. R. Munoz, M. C. C. Dos Santos, G. S. Medeiros, A. Simionato, D. A. Nagaoka, E.A. T. De Souza, S. H. Domingues, G. J. M. Fechine, Tuning of Surface Properties of Poly (vinyl alcohol)/ Graphene Oxide Nanocomposites. Polymer Composites, Wiley, 2018, https://doi.org/10.1002/pc.24659.

[9] S. Nuriel, L. Liu, A.H. Barber, H.D. Wagner, Direct measurement of multiwall nanotube surface tension. Chemical Physics Letters **2005**, 404 (4-6): p. 263-266, DOI: 10.1016/j.cplett.2005.01.072.

[10] M. Q. Tran, J. T. Cabral, M. S. Shaffer, A. Bismarck, Direct Measurement of the Wetting Behavior of Individual Carbon Nanotubes by Polymer Melts: The Key to Carbon Nanotube-Polymer Composites. Nano Letters 2008. 8(9): p. 2744, DOI: 10.1021/nl801209g.

[11] M. Hribova, F. Rybnikar, J. Vilcakova, Interaction of Carbon Nanotubes with Some Polymers. Journal of Macromolecular Science, Part B 2011, 50(1), p. 16, https://doi.org/10.1080/00222341003609070.

[12] H. Qian, A. Bismarck, E. S Greenhalgh, M. S. P. Shaffer, Carbon nanotube grafted silica fibres: Characterising the interface at the single fibre level, Composites Science and Technology 2010. 70(2): p. 393, DOI: 10.1016/j.compscitech.2009.11.014.

[13] A. H. Barber, S. R. Cohen, H. D. Wagner, External and internal wetting of carbon nanotubes with organic liquids. Physical Review B 2005, 71(11), p. 115443, https://doi.org/10.1103/PhysRevB.71.115443.

[14] R. Kotsilkova, E. Ivanov, E. Krusteva, C. Silvestre, S. Cimmino, D. Duraccio, Evolution of rheology, structure and properties around the rheological flocculation and percolation thresholds in polymer nanocomposites. In: “Ecosustainable Polymer Nanomaterials for Food

Packaging" (Silvestre C, Cimmino S, Eds), Taylor & Francis Books, Inc., Ch.3 (2013)pp. 55-86, ISBN: 978-90-04-20737-0. http://www.crcnetbase.com/isbn/9789004207387

[15] R Kotsilkova. Thermoset nanocomposites for engineering applications, Smithers Rapra Publishing, 2007, pp. 1-326, ISBN: 978-1-84735-063-3

[16] V. Angelov, H. Velichkova, E. Ivanov, R. Kotsilkova, M-H. Delville, M. Cangiotti, A. Fattori, M. Otaviani, EPR and Rheological Study of Hybrid Interfaces in Gold-Clay-Epoxy Nanocomposites. Langmuir **2014**, 30 (44), 13411–13421, https://doi.org/10.3933/applrheol-27-24469.

[17] M. J. Ariza, E. Rodriguez-Castellon, M. Munoz, J. Benavente, Surface chemical and electrokinetic characterizations of membranes containing different carriers by X-ray photoelectron spectroscopy and streaming potential measurements: study of the effect of pH. Surf. Interf. Anal. **2002**, 34, 637, https://doi.org/10.1002/sia.1377.

[18] D. Parobek, H. Liu, Wettability of graphene. 2D Mater. **2015**, 2, 032001, DOI: 10.1088/2053-1583/2/3/032001.

[19] L. Kock-Yee, H. Zhao, Surface wetting: characterization, contact angle, and fundamentals. Springer, Verlag, 2016.

[20] F.M. Fowkes, Attractive forces at interfaces. Industrial and Engineering Chemistry 1964, (56), 40-52, https://doi.org/10.1021/ie50660a008.

[21] F.M. Fowkes, Calculation of work of adhesion by pair potential summation. Journal of Colloid and Interface Science 1968, 4, 493-505, https://doi.org/10.1016/0021-9797(68)90082-9.

[22] R.N. Shimizu, N.R. Demarquette, Evaluation of surface energy of solid polymers using different models. J. Appl. Polym. Sci. 2000, 76, 1831, https://doi.org/10.1002/(SICI)1097-4628(20000620)76:12<1831::AID-APP14>3.0.CO;2-Q

[23] A. Rudawska, E. Jacniacka, Analysis for determining surface free energy uncertainty by the Owen–Wendt method. Int. J. Adhes. 2009, Vol.29, No. 4, 451-457, DOI: 10.1016/j.ijadhadh.2008.09.008

[24] C. Rulison, Models for Surface Free Energy Calculation. KRÜSS, Technical note TN306e, 1999

[25] D. K. Owens, R. C. Wendt, Estimation of the surface free energy of polymers. J. Appl. Polym. Sci. 1969, 13, 1741–1747, https://doi.org/10.1002/app.1969.070130815

[26] E. A. Dos Santos, M. Farina, G. A. Soares, K. Anselme, Surface energy of hydroxyapatite and β-tricalcium phosphate ceramics driving serum protein adsorption and osteoblast adhesion. J. Mater. Sci. Mater. Med. 2007, 19, 2307–2316, DOI: 10.1007/s10856-007-3347-4.

[27] L. Schramm, Emulsions, foams, and suspensions: fundamentals and applications. Hoboken: Wiley 2005.

[28] R. Ivanova, R. Kotsilkova, Rheological study of poly(lactic) acid nanocomposites with carbon nanotubes and graphene additives as a tool for materials characterization for 3D printing

Application. Appl. Rheol. 2018, 28, DOI: 10.3933/ApplRheol-28-54014.

[29] G. Spinelli, P. Lamberti, V. Tucci, R. Ivanova, S. Tabakova, E. Ivanov, R. Kotsilkova, S. Cimmino, R. Di Maio, C. Silvestre, Rheological and Electrical Behaviour of Nanocarbon/poly(lactic) Acid for 3D Printing Applications. Composites Part B. **2019,** 167, 467–47, https://doi.org/10.1016/j.compositesb.2019.03.021.

[30] S. Wang, Y. Zhang, N. Abidi, L. Cabrales, Wettability and surface free energy of graphene films. Langmuir **2009**, 25(18) 11078-11081, https://doi.org/10.1021/la901402f.

[31] J-F. Dai, G-J. Wang, L. Ma, Ch-K. Wu, Surface properties of graphene: relationship to graphene-polymer composites. Rev. Adv. Mater. Sci. **2015**, 40, 60-71

[32] M. Sakai, T. Yanagisawa, A. Nakajima, Y. Kameshima, K. Okada, Effect of surface structure on the sustainability of an air layer on superhydrophobic coatings in a water-ethanol mixture. Langmuir **2009**, 25, 13-16, doi: 10.1021/la802763h.

[33] R. Paul, Functional Finishes for Textiles: Improving Comfort, Performance and Protection, Handbook of Elsevier, Woodhead Publishing, Cambridge, UK 2015.

HIGHLIGHTS

- Surface properties of mono-filler (GNP/PLA) and bi-filler (GNP/MWCNT/PLA) composites based on poly (lactic acid) (PLA) polymer with graphene nanoplatelets (GNP) and multiwall carbon nanotubes (MWCNTs) were investigated as varying the amount and ratios of the fillers.
- The MWCNTs added to GNPs affect differently the Isoelectric point (IEP) and Zeta potential depending on the filler ratios, this indicating for variations in the bi-filler dispersion.
- Better dispersion and more homogenous bi-filler GNP/MWCNT/PLA nanocomposites having stronger interfacial and inter-particle interactions were obtained compared to the monofiller GNP/PLA systems.
- The hybrid fillers, GNPs/MWCNTs, depending on the filler ratios are proposed as a new way for synergistically tuning of surface properties of the PLA films.

Declaration of interests

☒ The authors declare that they have no known competing financial interests or personal relationships that could have appeared to influence the work reported in this paper.

☐The authors declare the following financial interests/personal relationships which may be considered as potential competing interests: